Bursting in 2-compartment neurons: A case study of the Pinsky-Rinzel model

Amitabha Bose
Department of Mathematical Sciences
New Jersey Institute of Technology, Newark, NJ 07102
bose@njit.edu

Victoria Booth
Departments of Mathematics and Anesthesiology
University of Michigan, Ann Arbor, MI 48109
vbooth@umich.edu

CAMS Report 0405-05, Fall 2004
Center for Applied Mathematics and Statistics

CHAPTER 1

Bursting in 2-compartment neurons: A case study of the Pinsky-Rinzel model

Amitabha Bose
Department of Mathematical Sciences
New Jersey Institute of Technology, Newark, NJ 07102, USA
e-mail:bose@njit.edu

Victoria Booth
Departments of Mathematics and Anesthesiology
University of Michigan, Ann Arbor, MI 48109, USA
e-mail:vbooth@umich.edu

The two-compartment Pinsky-Rinzel model of a hippocampal CA3pyramidal neuron consists of electrically coupled soma and dendritic compartments, each with active ionic conductances. This model has been widely used in a variety of contexts, but little analysis has been performed on its bursting solutions. In this chapter, we provide a geometric framework to study the Pinsky-Rinzel model. Using a combination of analysis and simulations, we identify neuronal mechanisms responsible for certain salient features of the model such as burst initiation and somatic-dendritic ping-pong. Some of these mechanisms are then demonstrated in a conceptually simpler, two-compartment Morris-Lecar model.

1. Introduction

Neurons are spatially distributed, heterogeneous entities. Among other structures, a neuron has dendrites which collect inputs, a cell body called a soma where integration of these inputs occur, an axon for output of neuronal signals, and synapses where communication with other neurons occurs. Different parts of the neuron may contain different ionic channels with different gating kinetics. Due to these potential complexities, accurate modeling of electrical activity of neurons is a challenging endeavor. Three basic approaches have been considered. One is to model the neuron using par-

tial differential equations to explicitly capture the spatial dependence[1,2,3]. Another is to use ordinary differential equations to model the neuron as a multi-compartment cell where the compartments are coupled via gap junctions[4,5,6,7,8]. The third approach is to treat the neuron as a single-compartment, point neuron[9,10]. In choosing one of these approaches, one must balance the need for biological plausibility versus the need for mathematical rigor and understanding of underlying phenomena.

In this chapter, we shall focus on multi-compartment neuron models. Although these models have been used widely in computational modeling studies, little analysis of such models has appeared in the literature. Of particular interest to us is the development of analytic tools that can be used to better understand the dynamics that arise as the result of multiple compartments. Here, we will work primarily with the Pinsky-Rinzel (PR) model[5] which is a two-compartment reduction of a larger 19-compartment model developed by Traub et. al.[4] of a hippocampal CA3 pyramidal cell. An important reason to study the PR model is that it introduced a specific modeling formalism which has been adopted by many others in more recent modeling studies. Namely, Pinsky and Rinzel lumped relevant active currents into a single "dendrite" compartment and segregated these from other currents lumped into a "soma" compartment. Although simple in concept, Pinsky and Rinzel demonstrated that this lumped, simplified model could qualitatively, and to a large degree, quantitatively describe the dynamics of the larger Traub model.

In the PR model, the interplay of active ionic currents between both compartments generates a wide variety of firing patterns ranging from tonic spiking to complex bursting. These features also contribute to the difficulty one faces in analyzing the dynamics of the model. The main purpose of this chapter is to provide a geometric framework from which one can begin analysis of the PR and other multi-compartment models.

For our analysis, we have modified the PR equations to simplify the gating kinetic equations for some of the ionic conductances. In this chapter, after briefly reviewing the modified PR model, we focus on two salient features of the model. First, we will show using phase plane analysis how to understand burst initiation in the PR model. We do so by deriving and analyzing a reduced set of equations which are valid in the silent state of the burst. By understanding the mechanism for burst onset, we are also able to understand how to control the burst frequency. We then turn our attention to the dynamics of two-compartment bursting, known as somatic-dendritic ping-pong[11], whereby the two compartments alternately depolarize one an-

other throughout the burst. We consider how ping-pong can fail to occur and how the ping-pong pattern can change depending on the dynamics in each compartment. We conclude by applying some of the lessons learned from the PR model to a simpler two-compartment model where each compartment is modeled by the Morris-Lecar equations.

2. The Pinsky-Rinzel Model

2.1. *Equations and qualitative description of the complex burst*

The original Pinsky-Rinzel equations for the two-compartment pyramidal cell model consist of current balance equations for a soma and dendrite compartment that are connected by electrical coupling. The soma compartment contains inward sodium and outward, potassium delayed rectifier active currents. The dendrite compartment contains an inward calcium current, I_{Ca}, an outward, voltage-activated potassium current, I_{K-C}, and an outward, calcium-activated, potassium after-hyperpolarization current, I_{K-AHP}. The equations are of the form

$$\begin{aligned} Cv_s' &= I_s - \bar{g}_L[v_s - E_L] - \bar{g}_{Na} m_\infty^2(v_s) h[v_s - E_{Na}] \\ &\quad -\bar{g}_{K-DR} n[v_s - E_K] - g_{coup}[v_s - v_d]/p \\ Cv_d' &= I_d - \bar{g}_L[v_d - E_L] - \bar{g}_{Ca} s^2[v_d - E_{Ca}] - \bar{g}_{K-AHP} q[v_d - E_K] \\ &\quad -\bar{g}_{K-C}\chi(Ca)c[v_d - E_K] - g_{coup}[v_d - v_s]/[1-p] \end{aligned} \tag{1}$$

The variables v_s and v_d represent the somatic and dendritic membrane voltages in mV, respectively. Ca represents calcium concentration. While I_{K-C} is voltage-activated, its conductance is modulated by the function $\chi(Ca) = \min(Ca/250, 1)$, a saturation function for calcium concentration. The steady state activation function $m_\infty(v_s)$ is sigmoidal and is effectively 0 when the neuron is subthreshold, and 1 when the neuron is active. Maximal conductances are given by $\bar{g}_x$ in mS/cm^2 and reversal potentials by E_x in mV ($x = L$ leak, Na sodium, Ca calcium, $K-DR$ potassium delayed rectifier, $K-AHP$ potassium after-hyperpolarization and $K-C$ voltage-activated potassium). The parameters $I_s = 0.75$ and $I_d = 0$ μA/cm^2 are applied current terms to the soma and dendrite, respectively. The parameter $p = 0.5$ measures the percentage of the total area of the soma compartment, $g_{coup} = 2.1$ mS/cm^2 is the electrical coupling conductance and $C = 3$ μF/cm^2 is the membrane capacitance. See Ref. 5 for the h, n and q gating kinetic functions, the Ca^{2+} concentration equations and for parameter values.

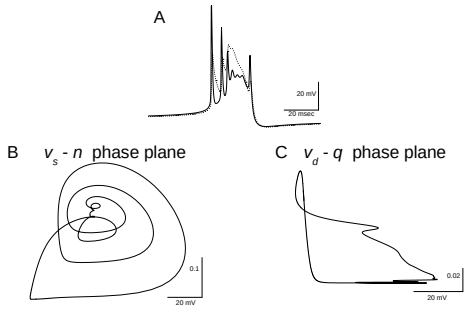

Fig. 1. Complex burst of the modified PR model. A: Somatic (solid curve) and dendritic (dotted curve) voltage trajectories. B,C: Burst trajectory projected onto the $v_s - n$ (B) and $v_d - q$ (C) phase planes.

The gating variables h, n and q in (1) obey first order differential equations of the form

$$y' = \alpha_y(U) - (\alpha_y(U) + \beta_y(U))y \tag{2}$$

where the argument U is v_s for $y = h, n$ and Ca for $y = q$. We have modified the equations governing the gating variables s and c for I_{Ca} and I_{K-C}, respectively, to the form

$$y' = [y_\infty(v_d) - y]/\tau_y(v_d). \tag{3}$$

The steady state activation functions $s_\infty(v_d) = 1/(1 + \exp(-(v_d + 20)/8))$ and $c_\infty(v_d) = 1/(1 + \exp(-(v_d + 10)/11))$ were fit to the corresponding functions in the original model. We simplified the time constant $\tau_s(v_d)$ to a constant $\tau_s = 2.535$ msec^{-1}. The time constant $\tau_c(v_d)$ was simplified to the piecewise linear function

$$\tau_c(v_d) = (1 - H(v_d + 10))\tau_{cc} + H(v_d + 10)(\tau_{cc} + 0.2(v_d + 10)) \tag{4}$$

where $H(v)$ is the Heaviside function. This simplification retains the break at $v_d = -10$ mV that appears in the original PR model but replaces the exponentially varying behavior for $v_d < -10$ mV with a constant $\tau_{cc} = 2.5$ msec^{-1}. The slope of $\tau_c(v_d)$ for $v_d > -10$ mV approximates the exponential behavior in the original model. The nullclines for all gating variables are sigmoidally shaped.

The modified PR model generates a complex burst essentially identical to the original model (Fig. 1). The burst is initiated by a sodium-mitigated spike in the soma compartment. This spike back-propagates and depolarizes

the dendrite compartment, activating the s, c and Ca variables. Calcium influx into the dendrite sustains dendritic depolarization which, in turn, provides sufficient depolarization through the electrical coupling to the soma to generate subsequent spikes. These subsequent spikes further depolarize the dendrite such that a partial dendritic calcium spike is induced. As a result, the soma is overdriven and the sodium spiking mechanism is shut down (depolarization block). Eventually, the burst ends when the calcium spike is shut off by I_{K-C} which builds up during the burst. The interburst length in this parameter regime, approximately 554 msec, is primarily governed by the slow decay of the potassium after-hyperpolarization gating variable q.

In Fig. 1, where we have projected the solution trajectory in the v_s-n and v_d-q phase planes, the direction of flow is counter-clockwise. Note that the trajectories in these phase planes intersect themselves, since these are projections of a higher dimensional flow onto two-dimensional phase planes. Phase plane analysis, as such, is not technically valid over all parts of the neuron's trajectory. However, as we will show below, it is possible to derive a set of simplified equations which govern subthreshold behavior of the neuron for which phase plane analysis is possible.

The PR model can also exhibit a wide variety of other firing patterns depending on parameter choices. These include tonic spiking in one or both compartments, mixed mode oscillations and aperiodic behavior. See Ref. 5 for more details.

One of the primary difficulties in analyzing the PR model is identifying which variables evolve on what time scales and over what parts of the cell's trajectory. The variables n and Ca decay slowly compared to all the other variables except for q which decays the most slowly. To analyze bursting, we will work with a set of slightly modified equations where we use a small parameter ϵ to demarcate fast and slow time scales. To derive them, we have broken the burst trajectory into four distinct regimes. The first is the jump up when somatic and dendritic voltages depolarize quickly at the leading edge of the burst. This occurs when $V_d^\star < v_d < v_\theta$ and $v_d' > 0$, where v_θ is some prescribed value and $V_d^\star$ will be described in detail in Section 3.1. The second regime is the active state of the burst where $v_d > v_\theta$. The third regime is the jump down when voltages repolarize at the end of the burst. In this state, $V_d^\star < v_d < v_\theta$, but $v_d' < 0$. The final regime is the silent state or interburst interval where $v_d < V_d^\star$. The modified equations that provide

for this dissection of the burst trajectory are:

$$\begin{aligned} v_s' &= F(v_s, n, h) - g_{coup}[v_s - v_d] \\ n' &= \epsilon[n_\infty(v_s) - n]/\tau_n(v_s, v_s') \\ v_d' &= f(v_d, q, Ca, s, c) - g_{coup}[v_d - v_s] \\ q' &= \epsilon\alpha(\nu Ca - q)/\tau_q(v_d, v_d') \\ Ca' &= \epsilon[-\mu\bar{g}_{Ca}s^2[v_d - E_{Ca}] - \beta Ca]/\tau_{Ca}(v_d, v_d') \\ s' &= [s_\infty(v_d) - s]/\tau_s \\ c' &= [c_\infty(v_d) - c]/\tau_c \\ h &= H(V_s^\star - v_s), \end{aligned} \tag{5}$$

The steady state activation functions n_∞, s_∞ and c_∞ are increasing sigmoidal functions which take values between 0 and 1, but whose values are assumed to be 0 when the neuron is silent. The following time constants take on the following values in the different states of the burst:

$$\tau_n(v_s, v_s') = \begin{cases} 1 & v_s > V_s^\star, \quad v_s' > 0 \\ \epsilon & v_s > V_s^\star, \quad v_s' < 0 \\ 1/\gamma & v_s < V_s^\star, \end{cases} \tag{6}$$

$$\tau_q(v_d, v_d') = \begin{cases} 1 \text{ during jump up, active state and silent state} \\ \epsilon \text{ during jump down,} \end{cases} \tag{7}$$

$$\tau_{Ca}(v_d, v_d') = \begin{cases} 1 \text{ during jump up and silent state} \\ \epsilon \text{ during active state and jump down,} \end{cases} \tag{8}$$

The parameters α, ϵ, γ, μ, ν, β, τ_s and τ_c are positive. The functions $F(v_s, n, h)$ and $f(v_d, q, Ca, s, c)$ denote the right hand sides of the v_s' and v_d' equations found in (1).

The above equations, while somewhat unwieldy, are in standard form to employ techniques of geometric singular perturbation theory. In particular, we can define relevant sets of reduced equations which will be the primary equations of interest. These equations are obtained by setting $\epsilon = 0$ in the above equations or in a rescaled version of them. Solutions of the reduced equations can then be pieced together to form a so-called singular solution. Using results of Ref. 12, for example, one can then prove that an actual solution to the ϵ small problem lies $O(\epsilon)$ close to the reduced solution. To this end, we shall work only with reduced equations.

3. Dynamics of the Pinsky-Rinzel model

In this section, we describe two important aspects of the PR model, burst initiation and somatic-dendritic ping-pong. These phenomena will be discussed geometrically using phase plane analysis. We also computationally

explore these issues where the effects of changing certain parameters can be addressed and illustrated.

3.1. *Burst Initiation*

With respect to burst initiation, an issue often addressed is how bursting oscillations arise as applied current to the neuron is increased. This has led to the classification of neurons as being Type I (those that are capable of arbitrarily low frequency oscillations) or Type II (those whose frequency is bounded from below)[13]. Here, we ask a different question. Once the neuron is in the bursting regime, what is the mechanism that allows the neuron to leave the silent state, i.e. what mechanism is responsible for the onset of each burst?

To understand how firing is initiated, we derive a set of reduced equations to describe dynamics in the silent state of the neuron when $v_d < V_d^\star$. These equations are obtained from (5) when time is rescaled with the new variable $\tau = \epsilon t$ and then ϵ is set to 0:

$$\begin{aligned} 0 &= F(v_s, n, 1) - g_{coup}[v_s - v_d] \\ \dot{n} &= -\gamma n \\ 0 &= f(v_d, q, Ca, s, c) - g_{coup}[v_d - v_s] \\ \dot{q} &= \alpha[kCa - q] \\ \dot{Ca} &= -bCa \\ 0 &= s \\ 0 &= c. \end{aligned} \tag{9}$$

In (9), differentiation is with respect to τ. We note that c and s act as parameters in the v_d equation, and that $s = 0$ reduces the Ca equation to a simple equation of exponential decay. There are three rate constants of interest in (9); α, γ and b. Of these, α is chosen to be substantially smaller than γ and b. Therefore, it is instructive to simplify (9) by assuming $n = 0$ and $Ca = 0$ in the silent phase. Thus equations (9) become

$$\begin{aligned} 0 &= F(v_s, 0, 1) - g_{coup}[v_s - v_d] \\ 0 &= n \\ 0 &= f(v_d, q, 0, 0, 0) - g_{coup}[v_d - v_s] \\ \dot{q} &= -\alpha q, \end{aligned} \tag{10}$$

with the algebraic equations for $Ca = s = c = 0$. The n-nullcline is the horizontal line $n = 0$. If $g_{coup} = 0$, the v_s nullcline of (9) would simply correspond to $F(v_s, n, 1) = 0$ which is a cubic shaped curve in the $v_s - n$ phase plane. It would not intersect the n-nullcline. However, when $g_{coup} \neq 0$, the

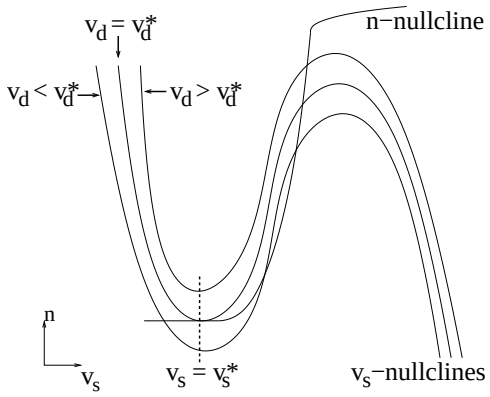

Fig. 2. The effect of v_d on the v_s-nullcline. A saddle-node bifurcation occurs when v_d increases through $V_d^\star$ thereby removing the two fixed points on the middle and left branch of the v_s-nullcline.

electrical coupling shifts this nullcline up or down depending on whether the quantity $I_{coup} \doteq g_{coup}(v_d - v_s)$ is positive or negative, respectively. If I_{coup} is sufficiently negative, the resulting cubic nullcline will intersect the n-nullcline, creating a fixed point in the $v_s - n$ subsystem. The existence of this fixed point prohibits the somatic trajectory from leaving the silent state. The quantity I_{coup} is continually changing during the silent state, however, since v_s and v_d are continually changing. Thus the v_s nullcline is a two-dimensional surface consisting of the left branches of raised and lowered cubics. There is a unique value $I_{coup}^* = g_{coup}(V_d^\star - V_s^\star)$ at which the fixed point disappears and a saddle-node bifurcation occurs (see Fig. 2).

This bifurcation occurs when the minimum of the v_s-nullcline is tangent to the n-nullcline. The value $V_s^\star$ satisfies

$$\partial F(V_s^\star, 0, 1)/\partial v_s - g_{coup} = 0, \tag{11}$$

while $V_d^\star$ satisfies

$$F(V_s^\star, 0, 1) - g_{coup}(V_s^\star - V_d^\star) = 0. \tag{12}$$

When $v_d < V_d^\star$, because of the fast v_s and n dynamics, equation (10) shows that v_s is always in a neighborhood of $V_s^\star$. Thus the condition that $I_{coup} = I_{coup}^*$ for a saddle-node bifurcation to occur, effectively reduces to $v_d = V_d^\star$. In turn, this yields a simple conclusion: if $v_d < V_d^\star$, there exists a fixed point of the fast $v_s - n$ subsystem and the v_s trajectory lies at this fixed point. If $v_d > V_d^\star$, there is no fixed point on the left branches of the v_s

nullcline and equations (9) and (10) are no longer valid. However, equations (5) and (6) then show that because of the fast v_s dynamics, the trajectory will leave a neighborhood of the left branches. Thus $V_d^\star$ provides a natural threshold for burst initiation. In short, if the trajectory is in the silent state, a burst will be initiated only when v_d increases through $V_d^\star$.

Pinsky and Rinzel[5] discuss that a burst is initiated when the variable q passes below a particular threshold. Equation (10) would appear to support this conclusion since q is the only dynamic variable in the silent state. However, we note that the values of $V_s^\star$ and $V_d^\star$ calculated from equations (11) and (12) are independent of q. While a value of q can be calculated at the moment of burst initiation, this value, in general, may change depending on the context. To elaborate, let us calculate the value of q at the bifurcation point using equation (10) for the v_d nullcline. When $g_{coup} = 0$, the graph of the v_d nullcline is a simple one-dimensional curve satisfying $f(v_d, q, 0, 0, 0) = 0$. When g_{coup} is non-zero, the v_d nullcline sweeps out a two-dimensional surface. In the silent state, however, v_s is always in a neighborhood of $V_s^\star$, so the v_d-nullcline is basically one-dimensional. At the bifurcation point, we find that $q = q_{bif}$ must satisfy $f(V_d^\star, q_{bif}, 0, 0, 0) - g_{coup}[V_d^\star - V_s^\star] = 0$. Using equation (1), we find that the value of q_{bif} satisfies

$$q_{bif} = \frac{-\bar{g}_L[V_d^\star - E_L] - g_{coup}[V_d^\star - V_s^\star]}{\bar{g}_{K-AHP}[V_d^\star - E_K]}. \tag{13}$$

For the set of parameters in Fig. 1, $q_{bif} = 0.155$. Note, however, that q_{bif} is inversely dependent on $\bar{g}_{K-AHP}$ indicating that a smaller value of $\bar{g}_{K-AHP}$ would allow q_{bif} to be larger. Figure 3 shows this situation. Here we show burst trajectories projected onto the $v_s - n$ and $v_d - q$ phase planes for $\bar{g}_{K-AHP} = 0.8$ mS/cm^2 as in Fig. 1 and for $\bar{g}_{K-AHP} = 0.6$ mS/cm^2. The trajectories of the soma and dendrite for the lower value of $\bar{g}_{K-AHP}$ are almost identical to those of Fig. 1, but now the value $q_{bif} = 0.207$ at burst initiation. Lower $\bar{g}_{K-AHP}$ also increases burst frequency because not as much $I_{K-AHP} = \bar{g}_{K-AHP} q[v_d - E_K]$ is activated and it has less of a hyperpolarizing effect on the v_d trajectory. As a result, v_d only spends a small amount of time below $V_d^\star$ and the interburst interval is shortened. Note that independent of the value of $\bar{g}_{K-AHP}$, the burst is initiated when v_d passes through $V_d^\star$ which in this case is around -52 mv. (see Fig. 3).

The value of q_{bif} can be made smaller at burst initiation when dendritic inhibition is applied during the interburst interval. Suppose that a term $-I_{syn} = -\bar{g}_{syn} s_{inh}[v_d - E_{inh}]$ were added to the right side of the v_d' equation

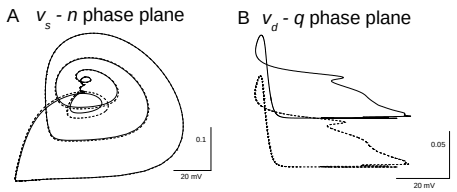

Fig. 3. Burst trajectories in the $v_s - n$ (A) and $v_d - q$ (B) phase planes for $\bar{g}_{K-AHP} = 0.8$ mS/cm^2 (dashed curve, default value) and 0.6 mS/cm^2 (solid curve).

in (1), (9) or (10). s_{inh} is a synaptic gating variable which, at the moment of a pre-synaptic spike (or burst), is reset to one and then decays like $\exp(-\kappa t)$ for some decay rate κ. As described in Ref. 14, inhibition causes the v_d nullcline to shift down in $v_d - q$ phase space and the v_d trajectory to hyperpolarize. Suppose that the neuron is in its silent state, and the time $t = 0$ is defined such that $v_d(0^-) = V_d^\star$. Next suppose that at $t = -t_{inh}$, for some small positive value t_{inh}, the dendrite receives an inhibitory input. This causes the value of v_d to decrease further away from $V_d^\star$, thus delaying burst onset (see Fig. 3B of Ref. 14). The burst will initiate at a time t_1 only after $s_{inh} = exp(-\kappa t_1)$ becomes sufficiently small. The time t_1 is dependent on the decay rate of inhibition. During the time interval $[0, t_1]$, q continues to decay independently of v_d according to the dynamics $q' = -\alpha q$ and thus can become smaller at burst onset (see Fig. 3B of Ref. 14 where $q_{bif} = .138$ for the uninhibited case and $q_{bif} = .12$ for the inhibited case). The analytic value of q_{bif} can be determined on a case-by-case basis and depends on the precise timing of the inhibition to the dendrites.

Although q does not set the threshold for burst onset, it can play a role in determining the interburst duration. Indeed for large values of $\bar{g}_{K-AHP}$, the decay constant α of the q variable strongly affects the interburst length. When $\bar{g}_{K-AHP}$ is too small, the v_d trajectory is barely pushed below $V_d^\star$, so the parameter α is less important in setting the interburst duration.

3.2. *Somatic-dendritic ping-pong*

One way to quantify ping-pong is to measure how the somatic firing pattern changes as the result of back-propagating spikes. In and of itself, the existence of the dendritic compartment is not sufficient to substantially change the somatic firing pattern. Rather an appropriate balance of the strength and timing of interactions of these two compartments is needed. Here we will be interested in a few different questions. What are some necessary con-

ditions for ping-pong to exist? When does ping-pong fail to exist? When ping-pong occurs, how is the somatic burst profile modulated?

A ping-pong burst generically refers to the ability of back-propagating spikes from the soma to exploit active properties of the dendritic compartment and thereby depolarize it. The depolarization of the dendrites subsequently causes depolarizing current to be re-injected to the soma and the process is given the chance to repeat. If it does, the soma and dendrite alternately depolarize one another a number of times before either outward currents put an end to the match or I_{coup} becomes too small.

Because of the electrotonic coupling between soma and dendrite, activity in one of the compartments instantly affects the other. Therefore ping-pong very much depends on the rates at which the individual compartments depolarize and hyperpolarize. Consider the parameters associated with the somatic compartment to be fixed. At the burst onset, the soma exhibits a sodium spike that then depolarizes the dendrite. The soma spike decays quickly. If the dendrite repolarizes too quickly, then it cannot return depolarization to the soma. Alternatively, if the dendrite does not repolarize quickly enough, then it can keep the soma depolarized too long, potentially overdriving the somatic spike generator. For ping-pong to occur, one compartment must be in a position in phase space to depolarize the other, and the other compartment must be in a position in phase space to be able to respond to the depolarizing current.

It is straightforward to derive a necessary condition for the cycle-by-cycle existence of ping-pong. Suppose the soma has spiked at time $t = 0$ and is now repolarizing, i.e. $v_s' < 0$. In order for the soma to depolarize again, there must exist a value $\hat{v}_1 > V_s^\star$ and a time t_1 such that $v_s(t_1) = \hat{v}_1$, $v_s'(t_1) = 0$ and $v_s''(t_1) > 0$. Using equation (5), we find that a necessary condition for ping-pong is $F(\hat{v}_1, n(t_1), 1) - g_{coup}[\hat{v}_1 - v_d(t_1)] \geq 0$ or

$$v_d(t_1) \geq \hat{v}_1 - \frac{F(\hat{v}_1, n(t_1), 1)}{g_{coup}}. \tag{14}$$

If, at a later time, the dendrite is repolarizing ($v_d' < 0$) then a necessary condition for ping-pong to continue is for there to exist $\hat{v}_2 > V_d^\star$ and a time t_2 such that $v_d(t_2) = \hat{v}_2$, $v_d'(t_2) = 0$ and $v_d''(t_2) > 0$. Again using (5), this translates to

$$v_s(t_2) \geq \hat{v}_2 - \frac{f(\hat{v}_2, q, Ca, s, c)|_{t=t_2}}{g_{coup}}. \tag{15}$$

A finite sequence of such values $(\hat{v}_i, t_i)$ can be generated. Each entry in the sequence would indicate the continuation of ping-pong for another cycle.

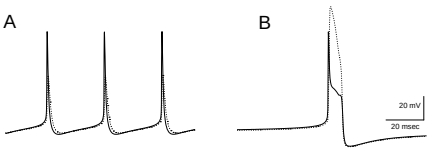

Fig. 4. Failure of ping-pong bursting in the modified PR model. A: Activation time constant τ_s for dendritic inward calcium current is increased to 10 msec^{-1} and dendrite repolarizes too quickly for ping-pong to occur. B: τ_s is decreased to 0.1 msec^{-1} and large dendritic spike is immediately initiated that overdrives soma. The dendrite remains depolarized too long to initiate ping-pong.

Equations (14) and (15) are instructive in several ways. First, they show that if g_{coup} is too small, then ping-pong is unlikely to occur. Note $F(\hat{v}_1, n(t_1), 1)$ and $f(\hat{v}_2, q, Ca, s, c)|_{t=t_2}$ are both negative implying that for small g_{coup}, $v_s(t_1)$ and $v_d(t_2)$, which are bounded from above, would need to be very large. Second, if g_{coup} is too large, then equations (14) and (15) cannot be satisfied. A large value of g_{coup} tends to make the v_s and v_d trajectories lie close together both in phase space and in time, thereby making $v_s - v_d$ small for any time t. Finally, although equations (14) and (15) do not pinpoint the values of $\hat{v}_1$ and $\hat{v}_2$ nor the times t_1 and t_2, together they provide some insights into the rates of de- and repolarization of the soma and dendrite needed to sustain ping-pong. For example, if equation (14) is satisfied, then for equation (15) to hold, the dendrite compartment cannot hyperpolarize too quickly, while the soma must depolarize sufficiently fast. Thus when applied current to either or both of the compartments is too large, thereby increasing these rates, ping-pong will fail to exist.

These ideas can be illustrated by varying the activation rate of the dendritic inward current I_{Ca}. This is controlled by the gating variable s and its associated time constant τ_s. In Fig. 4, we show two separate simulations in which we have changed τ_s to 10 (A) and 0.1 (B) msec^{-1}. In both cases, ping-pong fails. In the former (A), it fails because the activation rate is very slow and I_{Ca} is hardly activated. The dendrite is not depolarized beyond its response to the coupling current which deactivates very quickly. Thus the dendritic compartment repolarizes too quickly. The interburst length, approximately 30 msec, is still controlled by q, but q does not build up much. As a result, v_d spends little time below $V_d^\star$ and the frequency is relatively high. In the latter case (B), the calcium current activates very quickly and causes the v_d trajectory to stay in the active state for a relatively long time.

This, in turn, drives the v_s trajectory far above its spiking threshold. When the v_d trajectory ultimately repolarizes due to I_{K-C}, the v_s trajectory does so nearly simultaneously as well. Thus neither compartment is in a position to depolarize the other and ping-pong fails. Here q builds up quite a bit, so the interburst length, approximately 512 msec, is comparable to that of the complex burst.

In both of the above cases, ping-pong fails because one of the two compartments completely dominates the activity of the other. In the former (Fig. 4 A), the activity in the dendrites is slaved to that of the soma, and in the latter (B) the situation is reversed. This suggests that in order for ping-pong to work a proper balance in strength and timing of interaction between compartments needs to exist. Variations in this balance can lead to variations in the ping-pong pattern in which one compartment may have the upper hand during all or part of the burst.

In the PR complex burst (Fig. 1), the burst starts out with a true ping-pong between soma and dendrite. The initial somatic spike depolarizes the dendrite and partially activates I_{Ca} so that dendritic depolarization induces another soma spike. After the second spike, however, I_{Ca} activates more fully and the dendrite starts to dominate. The partial Ca^{2+} spike drives the soma into spike block, but as the dendrite repolarizes the soma is in a position to rejoin the game with a final small spike.

Keeping the soma parameters fixed, we can obtain variations on the ping-pong pattern by varying the activation time constants of I_{Ca} and I_{K-C}. For example, by slowing down the activation of the calcium current ($\tau_s = 2.55$ msec^{-1}) and speeding up the activation of I_{K-C} ($\tau_{cc} = 0.8$ msec^{-1}), true ping-pong bursting is obtained (Fig. 5A). In this case, the soma and dendrite alternately depolarize one another over four spikes. The interburst interval, approximately 165 msec, is shorter than in complex bursting since the low average dendritic depolarization doesn't allow much Ca^{2+} and, hence, q accumulation.

When the calcium activation rate is increased back to the same value as for complex bursting ($\tau_s = 2.535$) msec^{-1}and the I_{K-C} rate remains high ($\tau_{cc} = 0.8$ msec^{-1}), the soma and dendrite ping-pong over the first three spikes of the burst (Fig. 5B). Then a partial Ca^{2+} spike is generated and the dendrite dominates the game to the end of the burst. Here, the interburst interval, approximately 713 msec, is longer than in the basic complex burst because of the longer active state of the burst.

A dendrite-dominated burst occurs when the I_{Ca} activation rate is increased further ($\tau_s = 2$) and the I_{K-C} activation rate is decreased ($\tau_{cc} = 3$

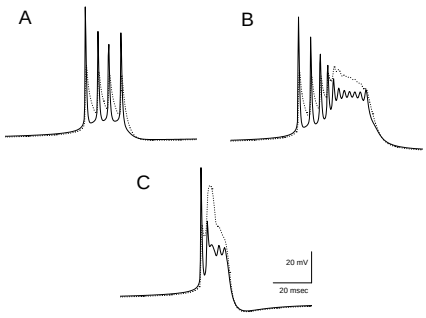

Fig. 5. Variations of ping-pong bursting in the modified PR model obtained by varying activation rates of dendritic calcium I_{Ca} and voltage-activated potassium I_{K-C}. Activation time constant τ_s of I_{Ca} set to 2.55 (A), 2.535 (B) and 2 (C) msec^{-1}. Parameter τ_{cc} of activation time constant $\tau_c(v_d)$ for I_{K-C} set to 0.8 (A),(B) and 3 (C) msec^{-1}.

msec^{-1}) (Fig. 5C). A larger Ca^{2+} spike is initiated immediately following the leading soma spike and it drives all further somatic activity. The interburst interval is long, approximately 689 msec, because the large Ca^{2+} spike increases Ca^{2+} and q accumulation.

Dendritic depolarization can also be modulated by external sources such as synaptic inhibition. In Ref. 14 (Fig. 6), we showed how different strengths of GABA-A mediated inhibition arriving at the dendrites just after burst initiation produces different types of firing patterns as well as different frequency bursting. Inhibition of moderate strength creates a balance between soma and dendrite which can allow ping-pong to exist over several cycles. Strong dendritic inhibition yields results similar to when $\tau_s = 10$ (Fig. 4A). Thus the effect of dendritic inhibition is very similar to the effect of changing the time constant τ_s for calcium influx.

4. Morris-Lecar two-compartment models

Ping-pong bursting can be studied more easily using a two-compartment model cell where each compartment is governed by the Morris-Lecar

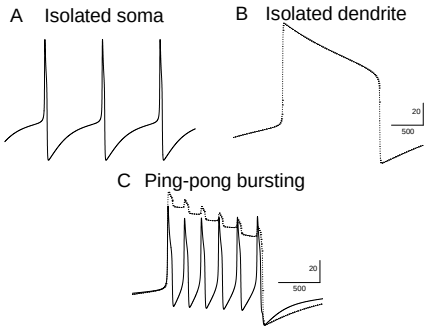

Fig. 6. Ping-pong bursting in the two-compartment Morris-Lecar model. Spiking trajectories in the soma (A) and dendrite (B) compartments when the compartments are uncoupled. Moderate strength coupling ($g_{coup} = 1$) results in ping-pong bursting (C, solid curve: somatic voltage, dotted curve: dendritic voltage).

equations[9]. The equations of interest are:

$$\begin{aligned} cv_s' &= I_s - g_{Ca} m_\infty(v_s)[v_s - E_{Ca}] - g_k w_s[v_s - E_K] \\ &\quad - g_l[v_s - E_L] - g_{coup}[v_s - v_d] \\ w_s' &= \phi[w_{s_\infty}(v_s) - w_s]/\tau_{w_s}(v_s) \\ cv_d' &= I_d - g_{Ca} m_\infty(v_d)[v_d - E_{Ca}] - g_k w_d[v_d - E_K] \\ &\quad - g_l[v_d - E_L] - g_{coup}[v_d - v_s] \\ w_d' &= \phi[w_{d_\infty}(v_d) - w_d]/\tau_{w_d}(v_d), \end{aligned} \tag{16}$$

where $c = 20$, $g_{Ca} = 4$, $g_k = 8$, $g_l = 2$, $E_{Ca} = 120$, $E_K = -84$, $E_L = -60$, $I_s = 40$, $I_d = 42$ and $\phi = 0.23$. The functions $m_\infty(v) = (1 + \tanh((v - v_1)/v_2))/2$, $w_{s_\infty}(v_s) = (1+\tanh((v_s - v_3)/v_4))/2$, $w_{d_\infty}(v_d) = (1+\tanh((v_d - v_5)/v_6))/2$, $\tau_{w_s}(v_s) = \tau_{lo,w_s} + [\tau_{hi,w_s} - \tau_{lo,w_s}]t_\infty(v_s)$, $\tau_{w_d}(v_d) = \tau_{lo,w_d} + [\tau_{hi,w_d} - \tau_{lo,w_d}]t_\infty(v_d)$ and $t_\infty(v) = (1 + \tanh((v - v7)/v8))/2$, where $v_1 = -1.2$, $v_2 = 18$, $v_3 = 12$, $v_4 = 17.4$, $v_5 = -8$, $v_6 = 10$, $v_7 = 12$ $v_8 = 17.4$, $\tau_{lo,w_s} = 30$, $\tau_{hi,w_s} = 10$, $\tau_{lo,w_d} = 100$ and $\tau_{hi,w_d} = 1000$.

For this set of parameters, when the compartments are isolated, $g_{coup} = 0$, the soma compartment fires single spikes with period 1907 units (Fig. 6A) and the dendrite compartment fires wide spikes with period 3355 (Fig. 6B). With sufficiently large g_{coup}, bursting is obtained and the burst is initiated when the v_s- and w_s-nullclines are tangent, thereby causing a saddle-node bifurcation as in the PR model. When $g_{coup} = 1$, the soma fires a burst of spikes as a result of its interaction with the dendrite compartment. The burst is initiated by a somatic spike that then activates the dendritic spike. The dendrite dominates the ping-pong dynamics, driving the subsequent

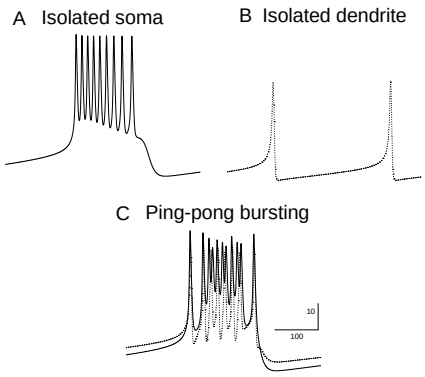

Fig. 7. Another example of ping-pong bursting in the two-compartment Morris-Lecar model. Isolated soma compartment displays bursting (A) and isolated dendrite repetitively spikes (B). Ping-pong bursting is obtained with moderate strength coupling $g_{coup} = 0.7$ (C, solid curve: somatic voltage, dotted curve: dendritic voltage).

somatic spikes. Here, the dendritic depolarization does not drive the soma into spike block, as can occur in the PR model. The burst width is shorter than the isolated dendritic spike since the repolarization of each somatic spike acts to slightly repolarize dendritic voltage. The burst period is 2906 units which is shorter than the isolated dendrite period, but longer than the isolated soma period. This makes sense since the burst is now being initiated by the soma trajectory as it passes through the saddle-node bifurcation as v_d passes through the threshold value $V_d^\star$. Here $V_d^\star$ is less than the value at which the isolated dendrite compartment would have become active. When $g_{coup} = 0.05$, the coupling is too weak for the dendrite to drive a burst of somatic spikes. With $g_{coup} = 10$, the coupling is too strong and both compartments have large burst envelopes, but no spiking behavior (simulations not shown). The advantage of using this simplified system is that it is easy to identify which parameters affect different parts of the burst oscillation. For example, τ_{lo,w_d} and τ_{hi,w_d} control the interburst duration and burst width, respectively.

Another example of ping-pong bursting can be obtained in the Morris-Lecar two-compartment model (see Fig. 7) if we modify the above equations using a trick found in Chapter 7.5 of Ermentrout's XPP book[15]. He shows that when the applied current of the basic Morris-Lecar equations satisfies a certain differential equation, the resulting solution exhibits a typical bursting pattern. We modified the above equations (16) to make I_s and I_d

obey the following differential equation:

$$I_x' = \epsilon[v_0 - v_x] \quad x = s, d, \tag{17}$$

with $v_0 = -26$ and $\epsilon = 0.001$. We also replaced the expressions for τ_{w_s} and τ_{w_d} with a common $\tau(v) = 1/\cosh((v - v_7)/(2v_8))$ where $v_7 = 12$ and $v_8 = 17.4$, and changed the parameters $v_5 = 7$, $v_6 = 17.4$. With these parameters, when the compartments are isolated, $g_{coup} = 0$, the soma compartment exhibits typical bursting (Fig. 7A), while the dendrite compartment fires tonically (Fig. 7B). With $g_{coup} = 0.7$, bursting is obtained and the burst is initiated through a saddle-node bifurcation of the soma compartment. The compartments engage in ping-pong, alternately depolarizing one another (Fig. 7C). The solution is not exactly periodic, but the basic phenomenon is consistent with what is seen in the PR model. The burst in this case ends at a homoclinic bifurcation when the average somatic and dendritic voltages dip below v_0. With stronger coupling, $g_{coup} = 10$, the compartments tonically spike at a frequency higher than that of the isolated somatic burst frequency. With $g_{coup} = 0.01$, there is no ping-pong as the coupling strength is too weak. For certain choices of parameters, ping-pong prolongs the length of the burst far beyond the homoclinic bifurcation point. This is because the average somatic and dendritic voltages during the burst are higher in the presence of coupling than without. Interested readers can see Fig. 7.9 of Ref. 15 for further elaboration.

5. Discussion

The Pinsky-Rinzel two-compartment model of a CA3 pyramidal cell has attracted wide interest in the neuroscience community. In part, this is due to its success in duplicating and explaining the dynamics of the larger 19-compartment model developed by Traub et. al[4]. Another reason is that it was one of the first models to show how active properties of the dendrites can affect the dynamics of the soma through the phenomenon of back-propagation of action potentials.

The PR model, and slight variations of it, have been used to address the dynamics of neocortical chattering neurons[11], the effect of different dendritic morphology on firing patterns[16], bistability in hippocampal pyramidal cell networks[17], rate, temporal and calcium coding[18,14], and patterns of burst synchrony[19]. Despite its wide usage, the PR model has been analyzed in limited cases [20,14] and has not been the subject of a rigorous mathematical treatment. In this chapter, we have begun the work of placing the PR model in a mathematical/geometrical framework suitable for analysis. By

focusing on burst initiation and the effects of back-propagation, we have provided some circumstances where the full PR equations (1) can be replaced by lower dimensional reduced equations for, at least, part of the cell's trajectory. In turn, this has allowed us to understand the mechanisms that are responsible for certain observed behaviors of the model. It also has allowed us to use this understanding to construct simpler models that exhibit effects of back propagation, but are much more transparent than the PR model.

With respect to burst initiation, we showed how changes in the coupling strength I_{coup} induce a saddle-node bifurcation in the fast v_s-n subsystem. This observation allowed us to understand through the reduced equations (10) how the length of the interburst is determined. Moreover, the analysis reveals that in any conductance-based two-compartment model, the strength of I_{coup} can affect the existence of fixed points in the silent state as well as the manner in which they disappear. For example, the phenomenon of ghost bursting, described by Doirnon et al [21,22], can be understood in the context of our analysis. Tonic firing in that model arises through a saddle-node bifurcation of fixed points as applied current I_s to the soma compartment increases through a value called I_{s_1}. For $I_s < I_{s_1}$, from our point of view, this means that the v_s and v_d trajectories are trapped at a fixed point, $(\bar{v}_s, \bar{v}_d)$ for which $\bar{v}_d < V_d^\star$. As I_s increases, $\bar{v}_d$ increases (due to current flow through the gap junction) while $V_d^\star$ decreases (a smaller value of v_d is needed to create the bifurcation since I_s is larger), until at I_{s_1}, $\bar{v}_d(I_{s_1}) = V_d^\star(I_{s_1})$. Thus when oscillations arise for I_s slightly larger than I_{s_1}, the fixed point $\bar{v}_d$ is only slightly larger in value than $V_d^\star$. Thus the time it takes for the v_d trajectory to cross $V_d^\star$ can become arbitrarily large since it is passing near a "ghost" of a fixed point. Thus the burst frequency can become arbitrarily small. This is what Doirnon et al mean when they talk about "reinjection near the ghost of a saddle-node point". The transition in their model from tonic firing to more complicated firing at $I_s = I_{s_2}$ appears to reflect the fact that the rates of de- and hyperpolarization of the soma compartment depend on I_s. For $I_s < I_{s_2}$, back propagation fails to affect somatic spiking and thus the solution is a period 1 orbit (tonic firing). For $I_s > I_{s_2}$, back propagation has an effect on the soma trajectory, affecting where it resides in phase space, making the solution quasiperiodic. For larger values of I_s the solution again becomes tonic spiking, which is consistent with what we find using equations (14)-(15).

In general, we can relate the onset of oscillations arising through a saddle-node bifurcation as a result of a change in applied current to our

work by understanding what affects $V_d^\star$ and what causes v_d to increase through this value. Alternatively, if the applied current in a model is fixed such that oscillations exist, one finds that the burst is initiated as I_{coup} changes strength. When the voltage of one compartment is stuck near a fixed point, I_{coup} acts like an applied current to that compartment. Increases in I_{coup} due to increases in the other compartment's voltage can then have the effect of causing a bifurcation in the number of fixed points in the other compartment.

Our analysis also suggests a few necessary conditions for back-propagation to have an effect on the firing dynamics of the soma. First, in the active state of the neurons, the amplitude of coupling current I_{coup} must be sufficiently large. Thus compartments that are nearly homogeneous are unlikely to display ping-pong. Homogeneity can be achieved either by assigning similar intrinsic properties to each compartment, or by making g_{coup} large which would have the effect of making $|v_s - v_d|$ small. Compartments that are weakly coupled (g_{coup} small) are also not likely to display ping-pong. A second condition that appears to be necessary for these effects is that one of the compartments contains a depolarizing current which decays on a slower time scale in the active state. This property gives ping-pong the chance to begin. In the PR neuron, this role is played by the calcium current in the dendrites. The third condition, and the hardest to quantify, is that the rates of depolarization and hyperpolarization of the two compartments need to be properly balanced. These rates are affected not only by intrinsic properties of the compartments, but also by the coupling conductance g_{coup} and potential external synaptic inputs. Thus when I_s or I_d is too large, ping-pong is not likely since the rates of de- and hyperpolarization are too large. In another example, in the standard PR model, the reversal potential of potassium is chosen to be $E_K = -75$ mV. With this value, and $\tau_s = 2.535$, the model exhibits a complex burst. If E_K is lowered to -84 mV, bursting gives way to tonic spiking. The lower reversal potential of potassium increases the rate of hyperpolarization of the soma and dendrite, negating the effect of back-propagation. By understanding this basic concept, it is straightforward to restore the complex burst, and there are many different ways to do so. For example, changing the reversal potential of calcium from 80 to 112 mV yields ping-pong bursting with 3-spike bursts and a slightly higher increase ($E_{Ca} = 112.5$ mV) recovers the complex burst, even with $E_K = -84$ mV. In these cases, the dendrite does not hyperpolarize as quickly, and can initiate ping-pong. See also the work of Hahn and Durand[17] who discuss other effects of changing E_K in the PR

model.

In this chapter, we have laid the geometric groundwork to allow for further analysis of two-compartment neurons. There are many open problems to be considered. While we have provided some necessary conditions for the existence of ping-pong, we are still far from analytically describing the phenomenon. Providing sufficient conditions, together with a geometric description of its existence, remains an open and challenging problem. Another open problem is to understand burst initiation in circumstances where the dynamics of the soma compartment in the silent state are not so fast. In this case, the slow manifolds associated with the silent state of each of the compartments will both be two-dimensional and the simple condition $v_d = V_d^\star$ for burst initiation would need to be replaced with $v_d = V_d^\star(v_s)$. Analysis of multi-compartment models connected by synaptic excitation or inhibition is also needed. For example in a network of PR neurons coupled by excitation, the perfectly synchronous burst solution is unstable. An analytic proof of such for a one-compartment Morris-Lecar type neuron exists[23], where a nearly synchronous solution is shown to be stable. A proof for the full or modified PR equations would be welcome.

Acknowledgments

This work was supported, in part, by the National Science Foundation (DMS - 0315862 (AB, VB) and ADVANCE DBI - 0340687 (VB)).

References

1. W. Rall, Core conductor theory and cable properties in neurons, In: Handbook of Physiology 1, 39-97, American Physiological Society, Bethesda, MD. (1977)
2. R. FitzHugh, Impulses and physiological states in theoretical models of nerve membranes, *Biophys. J.* 1, 445-466 (1961).
3. J. Nagumo, S. Arimoto, and S. Yoshizawa, An active impulse transmission line simulating nerve axons, *Proc. IRL* 50, 2061-2070 (1960).
4. R. Traub, R. Wong, R. Miles and H. Michelson, A model of a CA-3 hippocampal pyramidal neuron incorporating voltage-clamp data on intrinsic conductances, *J. Neurophsyiol.* 66, 635-649 (1991).
5. P. Pinsky and J. Rinzel, Intrinsic and network rhythmogenesis in a reduced Traub model of CA3 neurons, *J. Comput. Neurosci.* 1, 39-60 (1994).
6. F. Nadim, Y. Manor, M. Nusbaum and E. Marder, Frequency Regulation of a Slow Rhythm by a Fast Periodic Input. *J. Neurosci.* 18, 5053-5067 (1998).
7. G. Wallenstein and M. Hasselmo, Gabaergic modulation of hippocampal population activity: Sequence learning, place field development, and the phase precession effect, *J. Neurophsyiol.* 78, 393-408 (1997).

8. C. Laing and A. Longtin, A two-variable model of somatic-dendritic interactions in a bursting neuron, *Bull. Math. Bio.* 64, 829-860 (2002).
9. C. Morris and H. Lecar, Voltage oscillations in the barnacle giant muscle fiber, *Biophys. J.* 35, 193-213 (1981).
10. C. van Vanvreeswijk, L. Abbott and G. Ermentrout ,When inhibition, not excitation synchronizes neural firing *J. Comput. Neurosci.* 1, 313-321 (1994).
11. X. Wang, Fast bursting and short-term synaptic plasticity: a model of neocortical chattering neurons, *Neurosci.* 89, 347-362 (1999).
12. E. Mishchenko, and N. Rozov, Differential Equations with Small Parameters and Relaxation Oscillators, New York: Plenum Press (1980).
13. J. Rinzel and G.B. Ermentrout, Analysis of neural excitability and oscillations, In: C. Koch, I Segev eds. Methods in Neuronal Modeling, MIT Press, Cambridge, MA 251-291 (1989).
14. V. Booth and A. Bose, Neural mechanisms for generating rate and temporal codes in model CA3 pyramidal cells, *J. Neurophysiol.* 85, 2432-2445 (2001).
15. G. B. Ermentrout, Simulating, Analyzing and Animating Dynamical Systems: A Guide to XPPAUT for Researchers and Students, Philadelphia: SIAM (2002)
16. Z. Mainen and T. Sejnowski, Influence of dendritic structure on firing pattern in model neocortical neurons, *Nature* 382, 363-366 (1996).
17. P. Hahn and D. Durand, Bistability dynamics in simulations of neural activity in high-extracellular-potassium conditions, *J. Comput. Neurosci.* 11, 5-18 (2001).
18. X. Wang, Calcium coding and adaptive temporal computation in cortical pyramidal neurons, *J. Neurophysiol.* 79, 1549-1566 (1998).
19. V. Booth and A. Bose, Burst synchrony patterns in hippocampal pyramidal cell model networks, *Network: Comput. Neur. Syst.* 13, 157-177 (2002).
20. A. Kepecs and X. Wang, Analysis of complex bursting in cortical pyramidal neuron models, *Neurocomput.* 32-33, 181-187 (2000).
21. B. Doirnon, C. Laing, A. Longtin and L. Maler, Ghostbursting: A novel burst mechanism, *J. Comput. Neurosci.* 12, 5-15 (2002).
22. C. Laing, B. Doirnon, A. Longtin, L. Noonan, R. Taylor and L. Maler, Type I burst excitability, *J. Comput. Neurosci.* 14, 329-342 (2003).
23. A. Bose, N. Kopell and D. Terman, Almost-synchronous solutions for mutually coupled excitatory neurons, *Physica D* 140, 69-94 (2000).